Spin-dependent transport in Fe-doped carbon nanotubes

Bin Wang,[1] Yu Zhu,[1,2] Wei Ren,[1] Jian Wang,[1,*] and Hong Guo[2]
[1]*Department of Physics, The University of Hong Kong, Pokfulam Road, Hong Kong, China*
[2]*Center for the Physics of Materials and Department of Physics, McGill University, Montreal, PQ, Canada H3A 2T8*
(Received 17 January 2007; revised manuscript received 11 April 2007; published 12 June 2007)

We report on a first principles calculation of spin-dependent quantum transport in Fe-doped single-wall carbon nanotube (CNT) junctions. For junctions of a pristine (9,0) CNT in contact with Fe-doped (9,0) CNT leads, the total current in parallel configuration of the moment is larger than that of antiparallel configuration under lower bias voltage. For higher bias voltages the opposite happens. A tunnel magnetoresistance ration as large as 40% is found at zero bias, it decays with bias, and eventually goes to negative values at larger bias. Similar results are obtained for junctions with pristine (10,0), (8,0) CNT in contact with Fe-doped (10,0) or (8,0) CNT leads. The spin-dependent transport features can be understood by analyzing microscopic details of the transmission coefficients.

DOI: 10.1103/PhysRevB.75.235415 PACS number(s): 72.15.Jf, 85.65.+h, 73.40.Cg, 71.15.Mb

I. INTRODUCTION

Understanding the physics of spin-dependent quantum transport in magnetic tunnel junction (MTJ) is extremely important for magnetic device application. MTJ is the key to nonvolatile random-access memory,[1] programmable logic,[2] and next-generation magnetic sensor.[3,4] Conventional MTJ is fabricated from multilayer structures where a thin nonmagnetic material is sandwiched between ferromagnetic metals such as Fe, Co, Ni, and their alloys.[5–11] Due to electronic structure of the ferromagnetic material, during a tunneling process the spin-up and spin-down electrons from the metal layers traverse the nonmagnetic tunnel barrier with different Fermi wave function. The electrical resistance of MTJ is therefore sensitive to the relative orientation of the magnetic moments of the ferromagnet metal, resulting to a tunnel magnetoresistance (TMR).[12] In particular, the tunnel conductance tends to be smallest when the orientations are opposite, so that MTJs behave as spin valves.[12–16] Experimentally, it is possible to control the orientation of magnetic moments by imposing an external magnetic field.[17,18]

More recently, TMR has been achieved experimentally in molecular scale MTJ devices.[19–21] Molecular MTJ is fascinating because it closely couples phenomena of magnetism, transport, and quantum chemistry so that rich device physics is expected. So far, one of the most interesting molecular MTJs is the carbon nanotube (CNT) MTJ (Refs. 19, 22, and 23), where a segment of CNT is contacted by magnetic metal leads. Reference 19 reported ~9% TMR for the CNT devices where leads are Co. A larger TMR of about 30% was reported in Ref. 22 where multiwall CNT is sandwiched between Co pads, and this TMR decays quickly to zero as a function of bias voltage. It is believed[22] that the main contribution to spin-dependent tunneling comes from the Co/CNT conjunction, while the multiwall CNT itself acts as a spin-ballistic waveguide. Oscillations of TMR from 17% to −7% as a function of gate voltage was reported in this kind of CNT MTJs.[24] On the theoretical side, Mehrez *et al.*[25] investigated spin-coherent quantum transport in single-wall CNT MTJ using a tight binding model. Their calculation showed that resistance is sensitive to the relative orientation angle of magnetic moments in the two ferromagnetic leads. When the angle is rotated from π, antiparallel configuration (APC), to 0, parallel configuration (PC), TMR as large as ~20% was found at low temperatures.

A very interesting theoretical study on CNT magnetism was reported by Yang *et al.*[26] By filling and coating a different amount of Co and Fe atoms to the single-wall CNTs, magnetism of this hybrid structure was investigated. Because of a strong interaction between the ferromagnet and carbon atoms, spin polarization was found to be not sensitive to different hybrid structures. The *ab initio* calculations of Yang *et al.*[26] suggest that CNT doped with magnetic atoms can have substantial magnetic property and these doped CNTs can provide large spin polarization as large as 90%. In fact, CNTs filled with transition metal or ionic crystals were reported experimentally a long time ago.[27] Using the arc-discharge method, Guerret-Plecourt *et al.* filled nanotubes with more than 15 different metals and their compounds, such as Ti, Fe, and Co, etc. The experiment of Tsukagoshi *et al.* has shown[19] that CNTs can have a spin coherence length as long as 130 nm and even more. These findings suggest that CNTs may well become interesting for molecular magnetic devices. It is the purpose of this paper to theoretically exploit this possibility.

In particular, we consider a device where a segment of pristine single-wall CNT is contacted by two semi-infinite CNT leads which are doped with magnetic atoms, shown schematically in Fig. 1(a). We carry out first principles analysis of nonlinear spin-dependent quantum transport using a state-of-the-art atomistic technique based on density functional theory (DFT) in combination with Keldysh nonequilibrium Green's functions (NEGF).[28,29] The results show that for a pristine (9,0) CNT in contact with Fe filled (9,0) CNT leads, a TMR of 40% is obtained. As a function of bias voltage, the TMR can become negative. Similar results are obtained for (10,0) and (8,0) CNTs in contact with Fe-doped CNT leads. The spin-dependent transport features can be understood by analyzing microscopic details of the transmission coefficients.

The remainder of the paper is organized as follows. In Sec. II, the device structure and methods are presented. Section III presents results and Sec. IV is for a short summary.

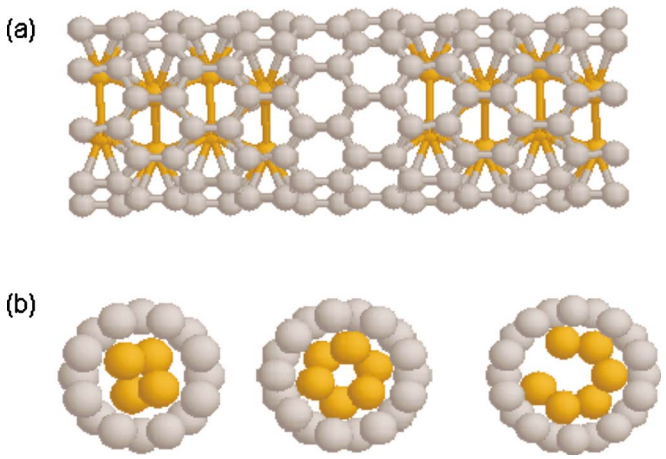

FIG. 1. (Color online) (a) Schematic plot of a CNT MTJ where a pristine (9,0) single-wall CNT is connected with the left- and right-hand CNT leads. The CNT leads are themselves (9,0) single-wall CNTs but they are doped with Fe atoms. (b) Unit cell cross sections of an (8,0) CNT filled with four Fe atoms; (9,0) CNT filled with six Fe atoms; and (10,0) CNT filled with six Fe atoms.

II. STRUCTURE AND CALCULATION METHOD

The CNT MTJ we studied is schematically shown in Fig. 1(a), where a pristine $(n,0)$ single-wall CNT is connected with $(n,0)$ CNT leads doped with Fe atoms. Due to magnetic properties of the doped CNT leads,[26] in the following we show that this system behaves as a spin valve.

In our analysis of the CNT MTJ in Fig. 1(a), one (or two, see next section) unit cell of pristine (9,0) CNT is connected with Fe-doped (9,0) CNT leads on the left- and right-hand sides. The length of the sandwiched pristine (9,0) CNT is 4.261 Å and the Fe-doped (9,0) leads extend to $z=\pm\infty$ where bias voltage is applied and spin-polarized currents collected. The cross sections of the leads are shown in Fig. 1(b). For a unit cell of (8,0) CNT lead, four Fe atoms are doped inside; for (9,0) and (10,0) CNT lead, six Fe atoms are doped, forming an *ABAB* staggered triangle packing. All the device structures were obtained by total energy relaxation using the SIESTA electronic package[30] in which nonlocal norm-conserving pseudopotentials are used to define atomic cores and a linear combination of numerical pseudoatomic orbitals to describe valence electrons. The cutoff radius for the pseudopotential of C atoms is set to 0.66 Å and the pseudopotential of Fe atoms is the same as that used in Ref. 31. Throughout the relaxation of structure, a conjugate gradient method was used until the residue force on each atom was less than 0.05 eV/Å. SIESTA calculation shows that the bond length of nearest Fe and C for Fe4-doped (8,0) CNT, Fe6-doped (9,0) CNT, and Fe6-doped (10,0) CNT are 2.236 Å, 2.146 Å, and 2.194 Å, respectively. For transport analysis, the magnetic moment orientation in the left-hand lead is fixed along the z axis while for the right-hand lead it is varied between parallel and antiparallel to the z axis.

To calculate spin-dependent transport properties, we make use of the first principles quantum transport package MATDCAL[28,29] where DFT is carried out within the Keldysh nonequilibrium Green's function formalism. The basic principle and practical implementation of the NEGF-DFT formalism can be found in Ref. 32. Essentially, within NEGF-DFT the device Hamiltonian and electronic structure are determined by DFT, the nonequilibrium quantum statistics of the device physics is determined by NEGF, and the transport boundary conditions under external bias are handled by real space numerical techniques. In our calculations, an s, p, d LCAO basis[30] set is used, atomic cores are defined by standard nonlocal norm conserving pseudopotential,[33] the exchange correlation is treated at the LSDA level.[34] The NEGF-DFT self-consistency is controlled by a numerical tolerance of 10^{-4} eV.

The spin-current (spin-polarized charge current) is calculated[15] as

$$J_\sigma(V) = \int_{-\infty}^{\infty} T_\sigma(E,V)[f(E-\mu_L) - f(E-\mu_R)]dE, \quad (1)$$

where f is the Fermi-Dirac distribution, $\mu_{L,R}$ are the chemical potentials of the left-hand (L) and right-hand (R) leads. $T_\sigma(E,V)$ is the transmission coefficient for spin channel $\sigma = \pm 1$ $(\uparrow,\downarrow)$ at energy E and bias voltage V. $T_\sigma(E,V)$ is obtained from NEGF as[15]

$$\mathcal{T}_\sigma(E,V) = 4[\mathrm{Im}(\Sigma_L^r)G^r\,\mathrm{Im}(\Sigma_R^r)G^a]_{\sigma\sigma} \quad (2)$$

and

$$T_\sigma(E,V) = \mathrm{Tr}[\mathcal{T}_\sigma(E,V)], \quad (3)$$

where the trace is over the basis functions. Here G^r is $2n \times 2n$ NEGF matrix where 2 is due to spin and n is the size of the basis set; Σ^r is the self-energy describing the coupling between the semi-infinite ferromagnetic leads and the scattering region which includes pristine CNT segment and two parts of Fe-doped CNT leads. For our system, Σ_L^r is diagonal and given by

$$\Sigma_L^r(E) = \begin{pmatrix} \Sigma_{L\uparrow}^r(E) & 0 \\ 0 & \Sigma_{L\downarrow}^r(E) \end{pmatrix}.$$

For parallel configuration, Σ_R^r is the same as Σ_L^r except changing subscript L to R. For antiparallel configuration, Σ_R^r is expressed as

$$\Sigma_R^r(E) = \begin{pmatrix} \Sigma_{R\downarrow}^r(E) & 0 \\ 0 & \Sigma_{R\uparrow}^r(E) \end{pmatrix}.$$

A more general form of the self-energy, accounting for noncollinear configuration, can be found in Refs. 15 and 25. In this work, only collinear moments are considered. In addition, due to the short length (~4 Å, see also the next section) of the pristine CNT barrier, spin-flip terms are neglected in the calculation. Finally, according to the prescription in Refs. 35 and 36, the spin-orbit coupling parameter δ is estimated to be $10^{-3} < \delta < 10^{-2}$ for graphite systems[36] which is small enough to be safely neglected.

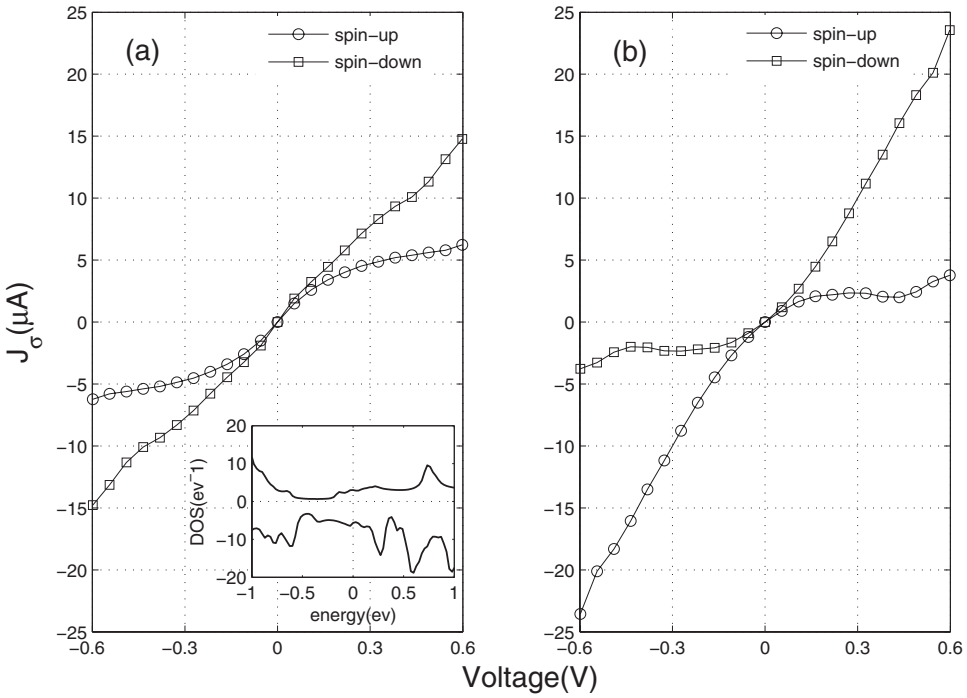

FIG. 2. (a) Spin currents $J_\uparrow$ (circles) and $J_\downarrow$ (squares) versus bias voltage in PC, for Fe-filled (9,0) CNT MTJ. Inset: DOS of the Fe-filled (9,0) lead. The upper curve represents the spin-up channel and the lower curve represents the spin-down channel. (b) Spin currents in APC.

III. RESULTS

In the inset of Fig. 2(a), which shows density of states (DOS) of an infinitely long Fe6-doped (9,0) CNT, a pronounced spin-polarization is clearly seen. Very near the Fermi level, the spin-down channel has more DOS. These are consistent with what was found before.[26] The main figure in Fig. 2(a) shows spin-current J_σ for the (9,0) CNT MTJ (see Fig. 1) versus bias voltage when the magnetic moments of the two leads are parallel (bias is applied to the right-hand lead). In this case, the value of $J_\downarrow$ (squares) is greater than $J_\uparrow$ (circles). The situation is different for APC, shown in Fig. 2(b), where $|J_\downarrow| < |J_\uparrow|$ for negative bias while the opposite happens for positive bias. This behavior may be attributed to DOS of both leads. For PC, the DOS of spin-down is always greater than that of spin-up among the range of bias voltages in Fig. 2, therefore $|J_\downarrow| > |J_\uparrow|$. For APC and negative bias, the DOS of spin-down spin is lower so that $|J_\downarrow| < |J_\uparrow|$, but for positive bias it is the other way around.

In Fig. 3(a) we present the conductance of Fe6-doped (9,0) CNT MTJ for both PC (squares) and APC (circles) as a function of bias voltage. In PC, a large equilibrium conductance of $2.7G_0$ is found, where G_0 is the conductance quanta, $G_0 = 2e^2/h$. This conductance value is larger than that of the pristine (9,0) CNT, which gives only $2G_0$ at Fermi level. That is because there are more than two bands at the Fermi level of the Fe6-doped (9,0) CNT, which serves as leads of the device, rather than only two bands for a pristine (9,0) CNT. In addition, the center region of the MTJ has only a very short segment of CNT, thereby many incoming channels can contribute to conduction resulting to a conductance greater than $2G_0$. The bias dependence of the conductance in Fig. 3(a) can be understood by consulting the behavior of J_σ versus bias in Fig. 2. At low bias, the total current $J = J_\uparrow + J_\downarrow$ in PC is greater than that of APC, therefore the conductance behaves the same way. As bias is increased, $J_\uparrow$ of Fig. 2(a) increases but its rate of increase goes down. This indicates a reduction of transmission coefficient by Eq. (1), consistent with the numerical result in Fig. 3 where conductance of the spin-up channel decreases as a function of bias. For APC, Fig. 2(b) shows that $J_\downarrow$ increases rapidly for increasing and positive bias, so that the total conductance of APC becomes a slowly increasing function of bias as shown in Fig. 3(a). Figure 3(b) plots TMR versus bias, where TMR is defined using the "pessimistic" definition

$$\mathrm{TMR} = \frac{J_{\mathrm{PC}} - J_{\mathrm{APC}}}{J_{\mathrm{PC}}}, \tag{4}$$

where J_{PC} and J_{APC} are total currents for PC and APC, respectively. At zero bias when all currents vanish, we compute TMR using equilibrium conductance. For the (9,0) CNT MTJ, TMR is found to decay from ~40% to zero and then to negative values when bias is increased. We now explain these behaviors in more detail.

To analyze the bias dependence of transport properties, we decompose transmission coefficients of Eq. (2) into contributions by all the eigenchannels of the device. These eigenchannels are obtained by diagonalization of $\mathcal{T}_\sigma$, where $\mathcal{T}_\sigma$ is the transmission matrix of the device scattering region. In our calculations the scattering region consists of the pristine (9,0) CNT segment plus two unit cells of the Fe-doped CNT lead on the left-hand and right-hand sides. By projecting all the scattering states onto these eigenchannels, we found that there are always several dominant eigenchannels that contribute to more than 98% of the total transmission coefficient. These are shown in Fig. 4 where the three panels on the left-hand column are projections for PC under three different bias voltages of 0.05, 0.27, and 0.49 volts, and those right-hand panels are for APC under the same bias. In each panel, curves on the upper half are projections for

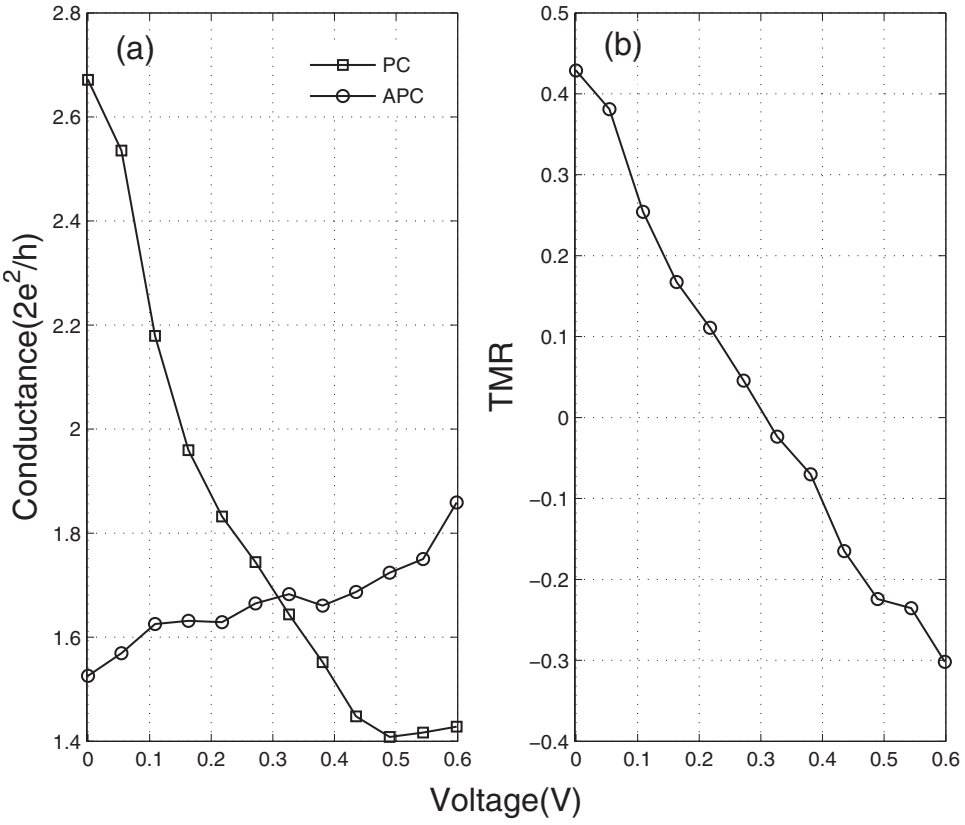

FIG. 3. (a) Total conductance of both spin-up and spin-down channels for Fe-doped (9,0) CNT MTJ versus bias voltage in PC (squares) and APC (circles). (b) TMR of the same device as a function of bias.

spin-up transmission and those on the lower half are for spin-down transmission. Using this definition only four dominating eigenchannels are shown in Fig. 4. This analysis finds that there are four eigenchannels contributing to $T_\uparrow$ near the Fermi level, but only one dominating channel is contributing away from it (the solid line). This is why the increase of $J_\uparrow$ slows down when bias voltage becomes large, already discussed above for Fig. 2(a). For APC at low bias, as shown in Fig. 4(d), there are three dominating eigenchannels contributing to both $T_\uparrow$ and $T_\downarrow$ near the Fermi level, but only one dominating eigenchannel away from it. When bias is larger [Fig. 4(f)], there is only one eigenchannel contributing to $T_\uparrow$

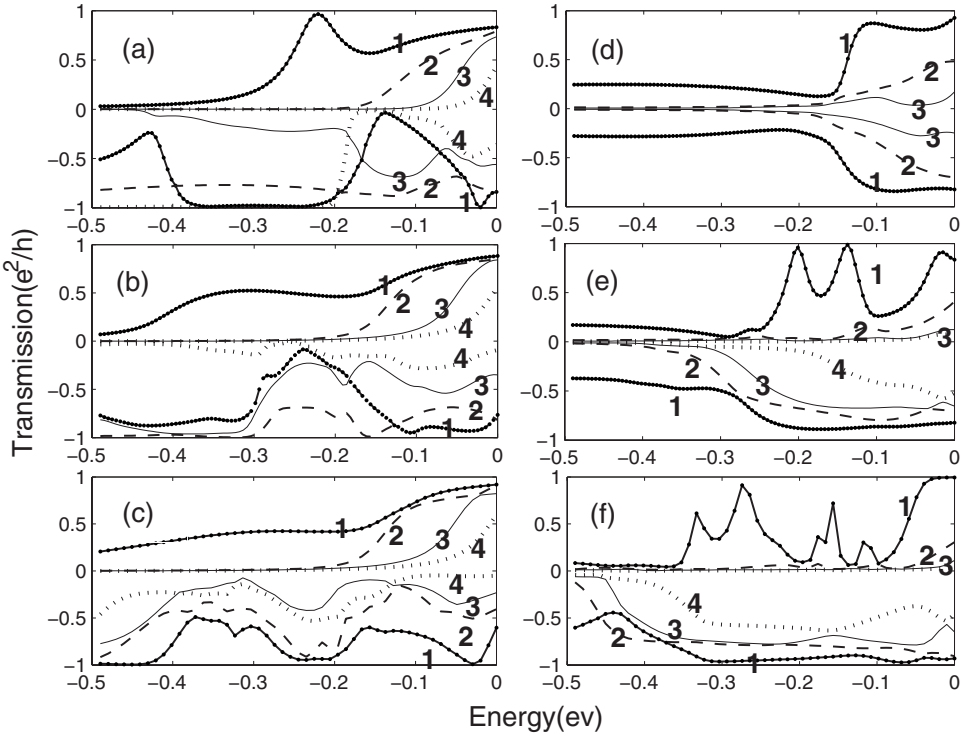

FIG. 4. Transmission coefficient of Fe-doped (9,0) CNT MTJ projected to every eigenchannel, as a function of energy. Left-hand panels are (a,b,c) are for PC and right-hand panels (d,e,f) are for APC. Bias voltages are 0.05 V for (a,d); 0.27 V for (b,e); 0.49 V for (c,f). Solid line, dashed line, dotted line, dashed-dotted line, and solid-dotted line are for different eigenchannels, which are labeled using numerals 1,2, 3,4 in all panels. The upper halves of each panel are for eigenchannels of spin-up transmission, the lower halves are for spin-down transmission.

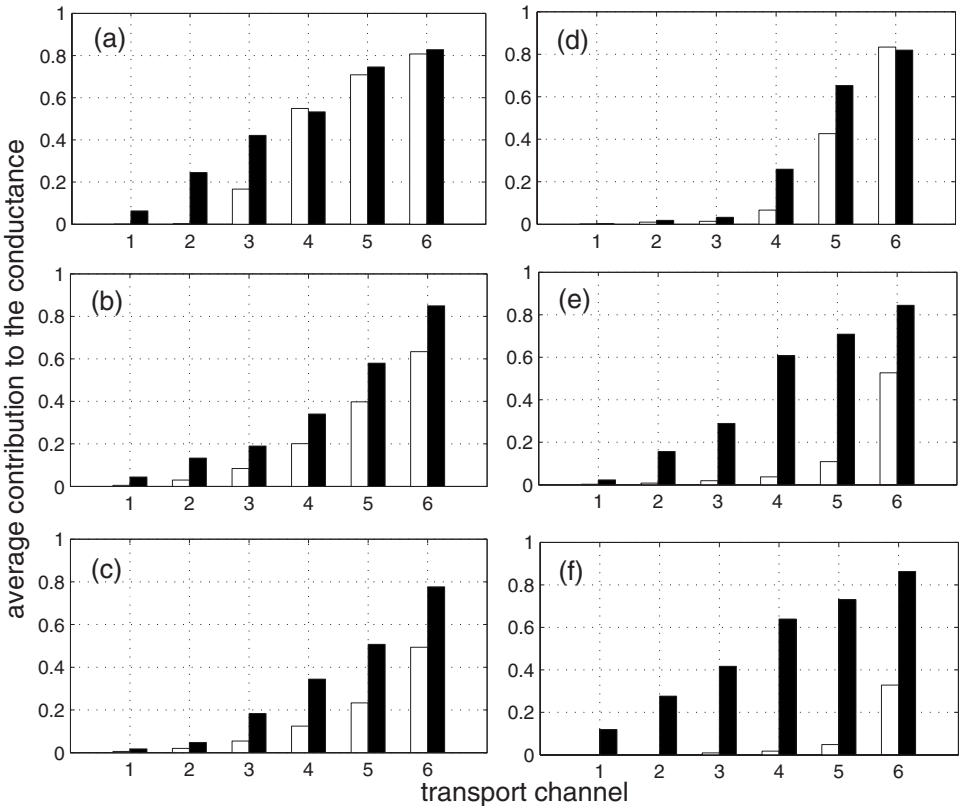

FIG. 5. Contribution to spin-current from six dominating eigenchannels which contribute more than 98% of the total. The left-hand panels (a, b, c) are for PC, right-hand panels (d, e, f) are for APC. Bias voltages are 0.05 V for (a,d); 0.27 V for (b,e); 0.49 V for (c,f). Empty bars represent contributions to spin-up current; filled bars to spin-down current.

but there are six eigenchannels contributing to $T_{\downarrow}$. Therefore for APC, $J_{\uparrow}$ is limited at larger bias but $J_{\downarrow}$ increases rapidly with bias as shown in Fig. 2(b).

Figure 5 plots a bar-chart representing contribution to J_{σ} from several dominating eigenchannels at three bias voltages. The bar height is obtained by Eq. (1) but replacing $T_{\sigma}(E,V)$ with partial transmission from each of the dominating eigenchannels. The three panels on the left-hand side are for PC and those on the right-hand side are for APC. For PC, the bar heights for spin-up (empty bars) contribution decrease rapidly with bias voltage, i.e., from Fig. 5(a) to Fig. 5(b) to Fig. 5(c). The bar heights for spin-down (filled bars) decreases relatively slower. Therefore, the total transmission (or conductance) decreases with bias in PC, as already seen in Fig. 3(a). The situation for APC is however different: the bar heights for spin-down (filled bar) actually increases with bias, giving rise to a slow increase of conductance versus bias as already seen in Fig. 3(a). Adding all the bar heights together, one obtains the total transmission coefficient at the three bias values. It is easy to verify by inspecting the left-hand and right-hand panels of Fig. 4 that conductance is much greater for PC than for APC at low bias [Figs. 4(a) and 4(d)], but it is the other way around for high bias [Figs. 4(c) and 4(f)], explaining the crossover behavior of the two curves in Fig. 3(a). At this crossover bias, by Eq. (4), we expect TMR to become negative. This is indeed what is obtained as shown in Fig. 3(b). Such a decaying TMR versus bias has been seen in many experiments in traditional planar MTJ (Refs. 10 and 11) as well as CNT MTJs.[23]

We have also investigated two other CNT MTJs made of (8,0) and (10,0) CNTs. When pristine, these are semiconducting tubes with a band gap. However, the Fermi energies of a pristine CNT and a Fe-doped CNT are rather different. When connected together, there is substantial charge transfer from the Fe atoms in the leads to the pristine CNT segment in the middle of the MTJ. Such a charge transfer shifts the Fermi level of the middle segment and, as a result, one may not obtain a semiconducting transport behavior at all. This indeed happens in the CNT MTJ as shown in Fig. 6. Figure 6(a) plots spin-current for Fe-doped (10,0) CNT MTJ versus bias in PC, and Fig. 6(b) for APC. The *I-V* curves do not show a semiconducting behavior due to the charge transfer. Similar metallic *I-V* characteristics are also found for Fe-doped (8,0) CNT MTJ [inset of Figs. 6(a) and 6(b)]. The metallic *I-V* behavior is consistent with the large transmission coefficients at the Fermi level, similar to that of Fe-doped (9,0) CNT MTJ. Detailed analysis has found that for the (10,0) MTJ, almost three charges are transferred from the Fe atoms in leads to the C atoms in the middle CNT, causing a realignment of the Fermi levels and giving rise to the observed metallic behavior.

Importantly, for both (10,0) and (8,0) MTJs, a clear TMR also exists. Figure 7(a) plots total conductance of Fe-doped (10,0) CNT MTJ versus bias for PC (squares) and APC (circles). The behavior is very similar to that of Fig. 3(a) for the (9,0) MTJ. We have also verified by analyzing the eigenchannels that the same physics as that of (9,0) MTJ is behind these *I-V* curves. As a consequence of this physics, a TMR $\sim$42% at zero bias is seen to decrease to about -15% as bias is increased, shown in Fig. 7(b). Finally, the inset of Fig. 7(a) plots total conductance of Fe-doped (8,0) MTJ where a crossover conductance between PC and APC is seen. Its

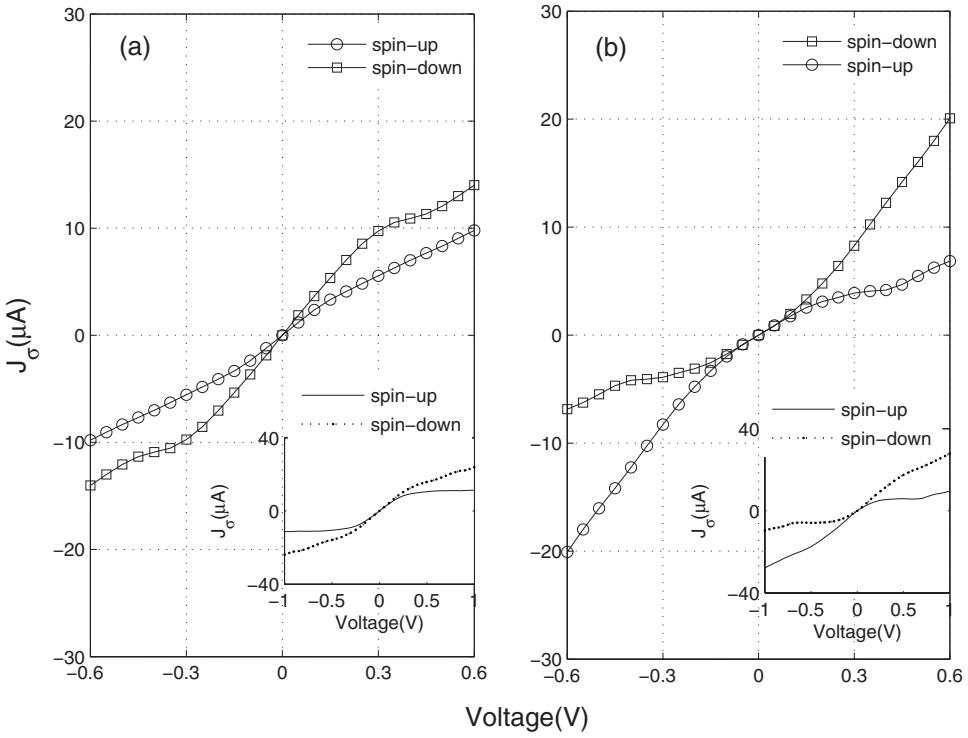

FIG. 6. Spin currents J_σ of Fe6-doped (10,0) CNT MTJ versus bias. (a) PC, (b) APC. Circles, $J_\uparrow$; squares, $J_\downarrow$. Insets in (a) and (b) are J_σ for Fe4-doped (8,0) MTJ for PC and APC, respectively. In the insets, the solid line is for $J_\uparrow$; the dotted line is for $J_\downarrow$.

TMR also decreases with bias all the way to negative values [inset of Fig. 7(b)]. These results are qualitatively similar as those for the (9,0) MTJ.

In order to examine the influence to TMR by the length of tunnel barrier, we have also examined a system with a longer pristine (9,0) CNT having two unit cells, sandwiched between the Fe-doped (9,0) leads. A qualitatively similar transport behavior was obtained as that of the shorter barrier MTJ. The conductance of PC decreases with the bias voltage while for APC it increases slowly. However, comparing to the shorter barrier MTJ, here the TMR ratio is somewhat smaller at zero bias which decreases from 0.32 to negative values and changes sign at around 0.5 V. This voltage scale is larger than that of the shorter barrier device where TMR changes sign at around 0.3 V. This result suggests that the decreasing rate of TMR is somewhat reduced with the increase of bar-

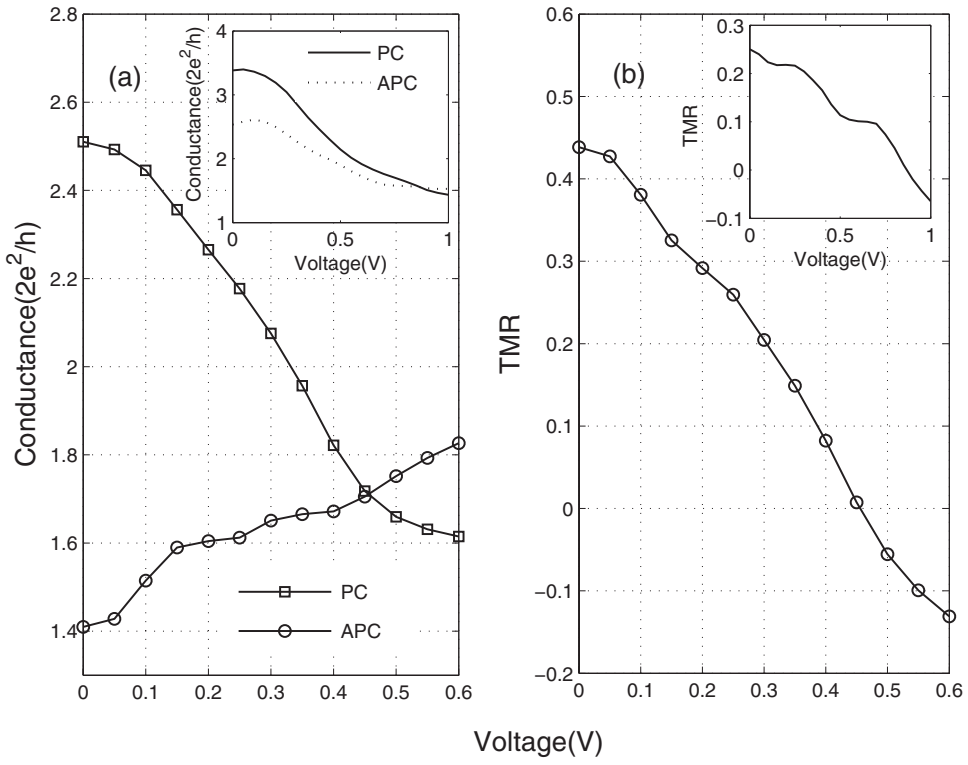

FIG. 7. (a) Conductance of Fe-doped (10,0) MTJ versus bias. Squares, PC; circles, APC. Inset of (a) plots conductance of Fe-doped (8,0) MTJ versus bias, solid line for PC, dotted line for APC. (b) TMR of Fe-doped (10,0) MTJ versus bias. Inset of (b) is TMR for Fe-doped (8,0) MTJ.

rier length. Finally, we note that it should also be interesting to investigate nonequilibrium features of multiwall CNT MTJ, although that would require extremely large computational effort.

IV. SUMMARY

Using a first principles technique based on NEGF-DFT, we have calculated spin-dependent quantum transport in Fe-doped single-wall CNT junctions. These junctions are shown to behave as MTJ with substantial TMR value. For the three different devices made of (8,0), (9,0), and (10,0) CNTs, the total conductance for PC is greater than that for APC at low bias, but the opposite happens at higher voltages. TMR is found to decrease with bias and eventually crosses over to negative values when APC current surpasses PC current. We have analyzed microscopic details of these transport features by projecting the spin-resolved transmission coefficients onto eigenchannels of the device at different bias voltages. It is found that only a few eigenchannels can contribute to more than 98% of total transmission. All the bias voltage dependent transport features of the device can be understood from the corresponding behavior of these dominating eigenchannels. The CNT based MTJs studied here suggest that CNT may well provide a useful route for realizing molecular spintronics.

ACKNOWLEDGMENTS

The authors thank Derek Waldron for his kind help with the Matdcal software package used in this work. Two of the authors (J.W., Y.Z.) were supported by RGC Grant No. HKU 7048/06P from the HKSAR and LuXin Energy Group; one of the authors (H.G.) acknowledges support by NSERC of Canada, FQRNT of Québec, and Canadian Institute of Advanced Research.

*Electronic address: jianwang@hkusub.hku.hk

[1] J. S. Moodera, L. R. Kinder, T. M. Wong, and R. Meservey, Phys. Rev. Lett. **74**, 3273 (1995); T. Miyazaki and N. Tezuka, J. Magn. Magn. Mater. **139**, L231 (1995).
[2] A. Ney, C. Pampuch, R. Koch, and K. H. Ploog, Nature (London), **425**, 485 (2003).
[3] E. Y. Tsymbal, O. N. Mryasov, and P. R. LeClair, J. Phys.: Condens. Matter **15**, R109 (2003).
[4] For a review, see, for example, I. Žutić, J. Fabian, and S. Das Sarma, Rev. Mod. Phys. **76**, 323 (2003).
[5] J. M. De Teresa, A. Barthelemy, A. Fert, J. P. Contour, R. Lyonnet, F. Montaigne, P. Seneor, and A. Vaures, Phys. Rev. Lett. **82**, 4288 (1999).
[6] E. Y. Tsymbal, A. Sokolov, I. F. Sabirianov, and B. Doudin, Phys. Rev. Lett. **90**, 186602 (2003).
[7] A. A. Tulapurkar, Y. Suzuki, A. Fukushima, H. Kubota, H. Maehara, K. Tsunekawa, D. D. Djayaprawira, N. Watanabe, and S. Yuasa, Nature (London), **438**, 339 (2005).
[8] T. Nagahama, S. Yuasa, E. Tamura, and Y. Suzuki, Phys. Rev. Lett. **95**, 086602 (2005).
[9] J. Nassar *et al.*, Appl. Phys. Lett. **73**, 698 (1998).
[10] S. S. P. Parkin *et al.*, Nat. Mater. **3**, 862 (2004).
[11] S. Yuasa *et al.*, Nat. Mater. **3**, 869 (2004).
[12] J. C. Slonczewski, Phys. Rev. B **39**, 6995 (1989).
[13] M. Julliere, Phys. Lett. **54A**, 225 (1975).
[14] A. M. Bratkovsky, Phys. Rev. B **56**, 2344 (1997).
[15] B. G. Wang, J. Wang, and H. Guo, J. Phys. Soc. Jpn. **70**, 2645 (2001).
[16] F. Mireles and G. Kirczenow, Phys. Rev. B **66**, 214415 (2002).
[17] J. Nowak and J. Rauluszkiewicz, J. Magn. Magn. Mater. **109**, 79 (1992).
[18] T. Yaoi, S. Ishio, and T. Miyazaki, J. Magn. Magn. Mater. **126**, 430 (1993).
[19] K. Tsukagoshi, B. W. Alphenaar, and H. Ago, Nature (London), **401**, 572 (1999).
[20] J. R. Petta, S. K. Slater, and D. C. Ralph, Phys. Rev. Lett. **93**, 136601 (2004).
[21] Z. H. Xiong, Di Wu, Z. Valu Vardeny, and Jing Shi, Nature (London), **427**, 821 (2004).
[22] B. Zhao, I. Monch, H. Vinzelberg, T. Muhl, and C. M. Schneider, Appl. Phys. Lett. **80**, 3144 (2002).
[23] B. Zhao, I. Monch, T. Muhl, H. Vinzelberg, and C. M. Schneider, J. Appl. Phys. **91**, 7026 (2002).
[24] S. Sahoo, T. Kontos, J. Furer, C. Hoffmann, M. Gräber, A. Cottet, and C. Schönenberger, Nat. Phys. **1**, 99 (2005).
[25] H. Mehrez, J. Taylor, H. Guo, J. Wang, and C. Roland, Phys. Rev. Lett. **84**, 2682 (2000).
[26] C. K. Yang, J. Zhao, and J. P. Lu, Phys. Rev. Lett. **90**, 257203 (2003).
[27] C. Guerret-Piëcourt, Y. Le Bouar, A. Lolseau, and H. Pascard, Nature (London) **372**, 761 (1994).
[28] D. Waldron, P. Haney, B. Larade, A. MacDonald, and H. Guo, Phys. Rev. Lett. **96**, 166804 (2006).
[29] D. Waldron, V. Timoshevskii, Y. Hu, K. Xia, and H. Guo, Phys. Rev. Lett. **97**, 226802 (2006).
[30] P. Ordejón, E. Artacho, and J. M. Soler, Phys. Rev. B, **53**, R10441 (1996); J. M. Soler, E. Artacho, J. D. Gale, A. García, J. Junquera, P. Ordejón, and D. Sánchez-Portal, J. Phys.: Condens. Matter **14**, 2745 (2002).
[31] C. C. Fu, F. Willaime, and P. Ordejon, Phys. Rev. Lett. **92**, 175503 (2004).
[32] J. Taylor, H. Guo, and J. Wang, Phys. Rev. B **63**, 245407 (2001); **63**, 121104 (2001).
[33] N. Troullier and J. L. Martins, Phys. Rev. B **43**, 1993 (1991).
[34] U. von Barth and L. Hedin, J. Phys. C **4**, 1629 (1972); O. Gunnarsson and B. I. Lundqvist, Phys. Rev. B **13**, 4274 (1976); A. K. Rajagopal, J. Phys. C **11**, L943 (1978).
[35] T. Ando, J. Phys. Soc. Jpn. **69**, 1757 (2000).
[36] A. Yanik, P. Srivastava, G. Klimeck, and S. Datta, 4th IEEC Conference on Nanotechnology, 2004.